A Compact Ultra-Wide Bandwidth Implantable Antenna for Leadless Pacemakers

Murray Brown supervised by Ismail Ben-Mabrouk

***Abstract*—This paper presents a 3x3x0.71 mm^3 implantable antenna for leadless pacemakers (LPs). Miniaturisation of the antenna is achieved through the use of a spiral meander pattern and a high dielectric constant superstrate and substrate, Rogers RT/duroid 6010. A shorting pin creates a second resonance which facilitates a wide simulated bandwidth of 20.0% operating in the industrial, scientific, and medical band (ISM: 2.4–2.5 GHz). The design and analysis of the antenna is carried out with simulation tools, based on the finite-element method. The peak gain of the antenna is -34.7 dBi and the calculated maximum specific absorption rate (SAR) values comply with IEEE C95.1-1999. A wireless communication link budget is calculated and the antenna is assessed at different implantation depths.**

I. Introduction

RECENT improvements in microelectronics technology have facilitated the introduction of a new generation of pacemakers with the potential to enhance patient quality of life. Pacemakers are an established therapy for the treatment of arrhythmias, with more than 1 million pacemakers implanted annually[1][2]. The ageing world population and increasing pacing indications mean the prevalence of pacemakers continues to increase [3][4]. Since the first implantation in 1958, there have been tremendous improvements in conventional pacemakers and their lead systems. However, 7-12% of patients experience complications within 6 months of implantation with conventional pacemakers. Most problems are related to a transvenous lead or a subcutaneous pocket [1]. Leadless Pacemakers (LPs) are proposed to reduce complications while simplifying procedures, allowing them to be safer, more cost-effective, and offer better patient quality of life [5]. LPs are typically inserted via a femoral vein transcatheter approach and attached to the inner heart wall. For wider adoption, LPs must overcome several challenges including multi-chamber pacing, battery longevity and device retrieval [6].

Biotelemetry in LPs allows for patient monitoring by healthcare professionals, typically by scheduled transmissions in between clinic visits [7]. This has the potential to improve device function and reduce unnecessary hospitalisation, increasing patient quality of life [7]. Alert transmissions can also notify physicians in near real-time [8]. Biotelemetry is achieved with an antenna in LPs which can send and receive signals. The frequency bands typically used for this communication are the industrial, scientific, and medical frequency bands (ISM) (433–435 MHz, 886–906 MHz, 2.4–2.5 GHz, 5.725–5.875 GHz), the medical implantable communication service frequency band (MICS), 402–405 MHz, and the wireless medical telemetry service frequency bands (WMTS) (608-614 MHz, 1.305-1.400 GHz, 1.427-1.432 GHz). Communication via Bluetooth low-energy (BLE) in the 2.4 GHz ISM band to patient-owned smartphones has been demonstrated to have a higher rate of scheduled transmission success than bedside monitoring devices [9]. This use is illustrated in Fig. 1(a). Fig. 1(b) shows the implantation of the pacemaker in the right ventricle (this is for illustration and is not to scale).

The limited space inside LP capsules, shown in Fig. 1(c), necessitates the miniaturisation of LP components. Current LPs (AVEIR, Micra, Nanostim) are in the region of a 6mm diameter and 25.9-41.4mm long [10][11]. The motivation for further miniaturisation of the components, including the antenna, is to reduce capsule size and improve battery life, telemetry and pacing.

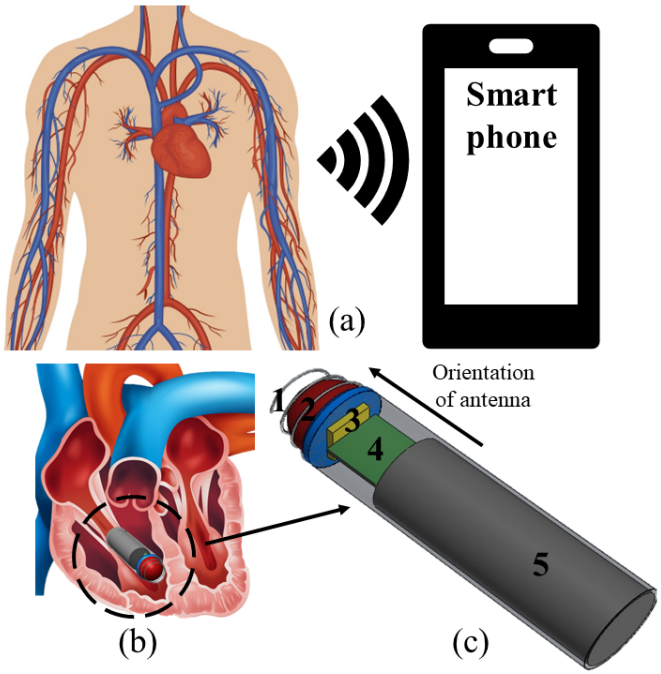

Fig. 1. Diagram of LP system (a) wireless transmission to smartphone (b) LP implant scenario (not to scale) (c) Proposed antenna in LP system model with components 1-5: fixation helix, electrode, antenna, circuit board, battery. (figures adapted from [12])

Significant research has been conducted into implantable antenna miniaturisation and performance. There are several parameters to assess the antenna including size, impedance matching, gain, bandwidth and Specific absorption rate (SAR).

[13] proposed a conformal 6x6x0.254 mm^3 antenna, which flexes to fit inside the LP capsule. It operates at 1.4 GHz and 2.45 GHz with a gain of -33.2 dBi, and -28.5 dBi, respectively. [14] realised miniaturisation with a conformal planar inverted-

f antenna (PIFA) which implemented power harvesting. The design had a 20.5x30x0.05 mm^3 (9.46 mm diameter) footprint with a realized gain value of -32 dBi. This design is larger than modern LP capsules. [15] presented a 6.578 mm diameter conformal antenna operating at 2.4 GHz with a realised gain of -35 dBi. These conformal antennas make good use of space as they wrap the inner capsule wall of the LP. However, they are difficult to integrate with internal circuitry. [16] made use of the diameter of the capsule with a centrally fed 6mm diameter spiral antenna, achieving a peak realized gain of -30.33 dBi and a bandwidth of 28 MHz. Other designs applied miniaturisation techniques to rectangular planar antennas [17] [18] [19] [20]. [17] introduced 2 symmetrical spiral meanders with a hooked ground plane slot in a 7x6.5x0.375 mm^3 footprint. It operated at 400 MHz 1.6 GHz and 2.45 GHz with gains of -30.5, -22.6 and -18.6 dBi respectively. [18] presented a 7x6x0.377 mm^3 design also employing a hooked open-end ground slot as well as a closed slot and a shorting pin to allow it to operate at 915 MHz, 1.4 GHz, and 2.45 GHz with gains of -28.7, -20.02, and -16.7 dBi respectively. The performance of the designs in [17] [18] came at the cost of size, as the designs would not fit into modern LP capsule sizes, like the Micra and Nanostim systems. [19] presented, a 3x4x0.5 mm^3 spiral meander which achieved a peak gain of -25.95 dBi and 21.8% bandwidth. A high dielectric constant substrate and superstrate were used to reduce antenna losses. The smallest design in the literature was a 3x3x0.5 mm^3 footprint. [20] used a folded meander with 5 open-end ground slots, achieving a gain of -24.9 dBi.

This paper proposes a novel 3x3x0.71 mm^3, ultra-wide bandwidth implantable antenna, using a shorting pin to enhance bandwidth for biotelemetry in LP systems. It is organised into the following sections. Section II explains the antenna design process and simulation setup. Section III details the performance characteristics of the antenna including reflection coefficient, gain, radiation efficiency, Specific Absorption Rate (SAR) and link budget. Section IV concludes the key findings and future research directions.

II. Methodology

A. Antenna Design

Fig. 2 presents a detailed model of the proposed spiral meander design. In antenna design, the length of the antenna is proportional to the resonant frequency. If our antenna operates as a quarter-wavelength monopole, we can apply the relationship:

$$L \approx \frac{c}{4f\sqrt{\epsilon_r}} \tag{1}$$

L is the length of the antenna, c is the speed of light in a vacuum, f is the operating frequency, and ϵ_r is the dielectric constant. Fig. 2(a) shows the radiating patch of the antenna. The meander acts to extend the length of the antenna to achieve miniaturisation within the small footprint. The design also includes a dielectric plate next to the feed, similar to [20]. After implantation into biological tissue, the effective dielectric constant changes compared to free space. The antenna materials also impact the effective dielectric constant.

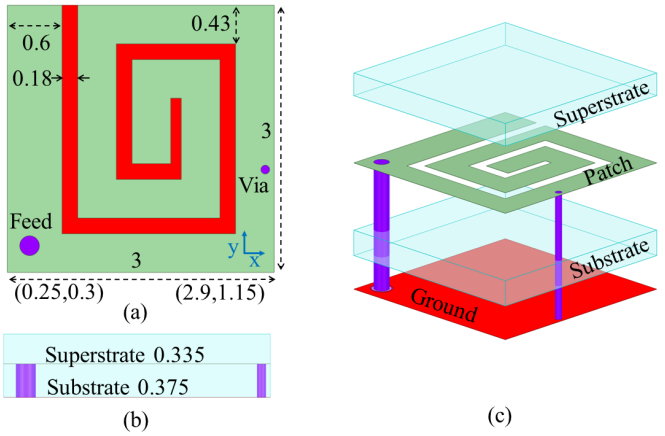

Fig. 2. Proposed spiral antenna structure (a) Radiating layer with position of feed and via (b) Side view (C) Exploded view (unit:mm)

A high dielectric constant superstrate changes the effective dielectric constant of the antenna's operating medium and shifts the resonant frequency to lower frequencies. This allows for a shorter antenna length for the same operating frequency. Rogers6010 was selected for the substrate and superstrate shown in Fig. 2(b) due to its high dielectric constant of 10.2 and tangent loss of 0.0023 s/m. Fig. 2(c) shows a view of the 50 Ω coaxial feed as well as the shorting pin (via), which creates a second resonance point to widen the bandwidth of the antenna. To the author's knowledge, shorting pins have not been presented in the literature in implantable antennas with patch sizes below 5×5 mm^2.

A key property of implantable devices is biocompatibility. This antenna is intended to be encapsulated in a biocompatible capsule. However, many authors suggest a biocompatible film should be added to the antenna [20] [19]. The antenna could be coated in a thin film of ceramic aluminium oxide for compatibility [21].

B. Simulation

The impacts of human tissue on the transmission of electromagnetic radiation are difficult to model analytically, especially for complicated antenna structures. Researchers can analyse implanted antenna performance within both simplified numerical models and anatomical models included in simulators such as Ansys High Frequency Structure Simulator (HFSS), which is based on the finite element method. Many different numerical models and simulation setups have been proposed by authors to simulate heart implantation [13] [14] [16][19]. This paper employs a 60x80x120 mm^3 homogeneous heart muscle phantom shown in Fig. 3 to mimic the size of a human heart [22]. The implantation depth is 10mm to approximate pacing of the right ventricle. The dielectric properties of heart tissue are frequency-dependent. A conductivity of 2.215 S/m and dielectric constant of 54.918 were used to model heart tissue at 2.45 GHz [23]. The simplicity of the model allows for faster optimisation calculations.

HFSS Optimetrics were used to optimise for peak gain at 2.45 GHz and reflection coefficient (S11) over the 2.4-2.5 GHz

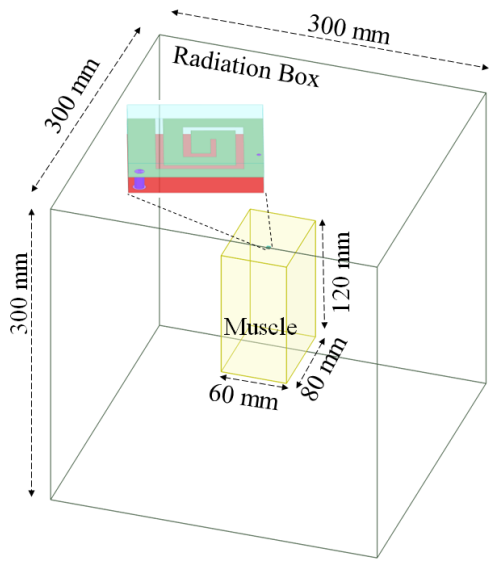

Fig. 3. Simulation set-up for optimisation in the homogeneous heart phantom within a radiation box.

operating band. The feed position, short position, meander width, meander gap width, and substrate and superstrate thickness were all optimised over 1000s of iterations.

III. Results and Discussion

Fig. 4 shows the S11 of the antenna. The simulated -10 dB fractional bandwidth of 20.0% extends from 2.2 GHz to 2.7 GHz- well beyond the 2.4-2.5 GHz ISM band. The wide bandwidth is due to the shorting pin extending the antenna resonance into higher frequencies. However, the response is not centred at 2.45 GHz as the lowest value of S11 is -30.26 dB at 2.5 GHz. The optimisation set-up attempts to satisfy both gain and impedance matching targets and as a result, the main resonance has shifted slightly. The wide bandwidth is desirable to maintain communication within the ISM band for implantation in different patients where tissues vary, which causes detuning effects. Additional bandwidth widening, as well as detuning, would be likely to occur in the measurement of a fabricated version of the proposed antenna, as observed in many of the cited designs [17][19][20][24]. Authors have suggested this is due to coupling either with other components of the LP device, or coupling with biological tissues not accounted for in the simulation.

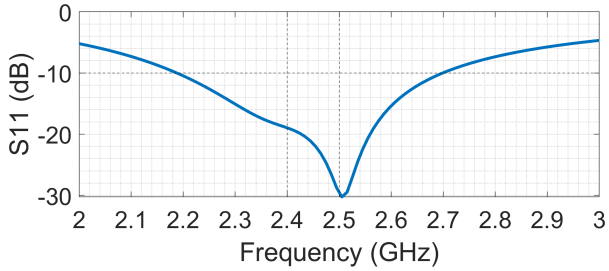

Fig. 4. S11 of proposed antenna in the homogeneous heart phantom over 2-3 GHz.

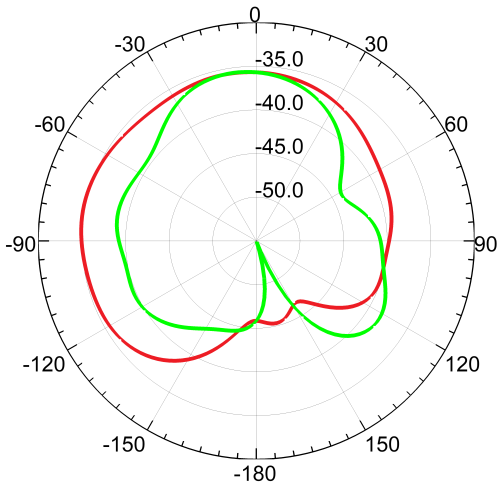

Fig. 5. Gain pattern at 2.45 GHz: red: E-plane, green: H-plane.

The radiation pattern of the antenna is presented in Fig. 5. The peak gain is shown to be -34.7 dBi. The radiation pattern is not omnidirectional. Relative high gain is observed where the phantom is shallow. Therefore, the radiation is directed out of the body for communication. The low gain in other directions will result in lower radiated energy absorption by the body, lowering SAR. Fig. 6 shows the current path at

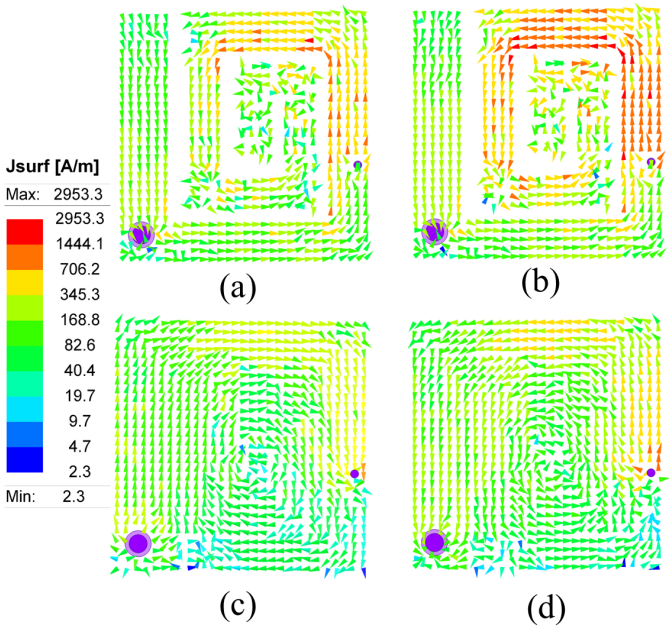

Fig. 6. The current distribution of the antenna (a) Patch at 2.3 GHz (b) Ground at 2.3 GHz (C) Patch at 2.5 GHz (D) Ground at 2.5 GHz.

2.3 GHz and 2.5 GHz to show the 2 operating modes of the antenna. Fig. 6(a) shows the current path at 2.3 GHz, where the current can be seen to flow in the same direction along the length of the meander. The current does not change direction and therefore, it is shown to act as a quarter-wavelength monopole [17]. Some current is seen to be contributed by the shorting pin path. This is because the 2 resonant points of the

antenna are close together, so each mode cannot be observed individually. Fig. 6(b) shows the current flow for 2.5 GHz where the shorting pin allows for much higher current flows along a shorter current path. The antenna operates as a shorter quarter-wavelength monopole between the shorting pin and the end of the meander. 6(b) and Fig. 6(d) show low current densities in most of the ground plane. However, there is high current density near the via in Fig. 6(d). The low current in the ground plane should reduce coupling between back radiations and the other components of the LP [24].

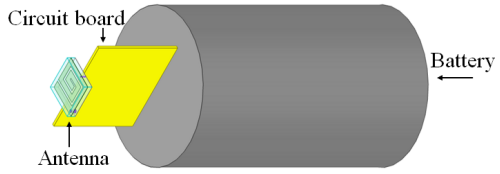

Fig. 7. LP component model.

Fig. 7 shows a model of LP components where the circuit board is modelled as Teflon and the battery is a perfect conductor. There is a 0.01 mm separation between the antenna and the circuit board. The orthogonal orientation of the antenna to the circuit board should reduce coupling. S11 and gain were simulated with the other components of the LP system and no change was observed.

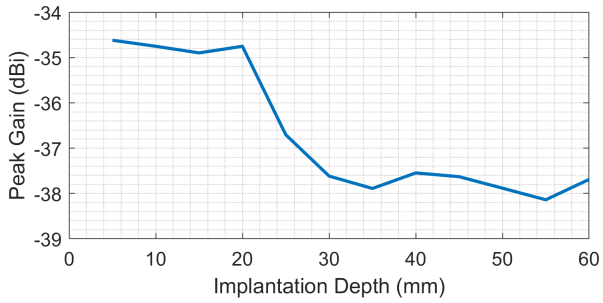

Fig. 8. Effects of implantation depth on peak gain.

Fig. 8 shows the impact of implantation depths between 5 mm and 60 mm on peak gain. Gain is shown to decrease with implantation depth however, the result is much more gradual than has been reported for similar footprints [20]. A peak gain of -37.8 dBi is shown for an implantation depth of 60mm. S11 was also assessed against implantation depth however little variation was observed. The proposed antenna peak gain, peak realized gain and radiation efficiency in the frequency range 2-2.8 GHz are shown in Fig. 9. Realised gain, gain and radiation efficiency all peak in the 2.4-2.5 GHz frequency band however, realised gain and gain peak at close to 2.5 GHz. The radiation efficiency and realized gain at 2.45 GHz are 0.015% and -35.1 dBi respectively. Low radiation efficiency in implantable antennas is due to the coupling of the antenna with human tissues. Radiation efficiencies of less than 1% are typical for implantable antennas [25]. However, The radiation efficiency of the proposed design is low compared to the literature.

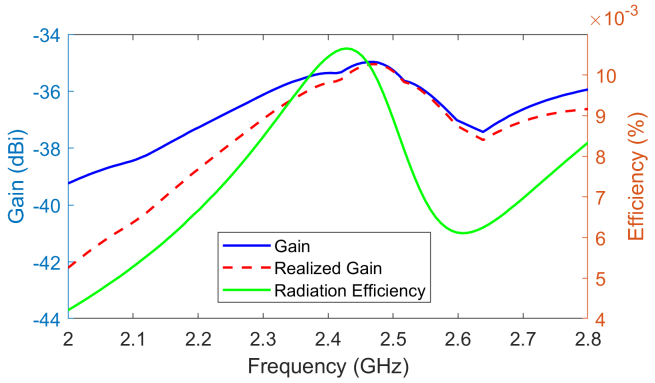

Fig. 9. Gain, realized gain and radiation efficiency vs. frequency.

Safety assessment is critical for implantable antennas to ensure radiation emitted into human tissues is within safe limits. The safety guidelines set by IEEE C95.1-1999 require the average specific absorption rate (SAR) in human tissue to not exceed 1.6 W/kg and 2 W/kg in 1 g of tissue and 10 g of tissue respectively. The European Research Council regulation stipulates a maximum allowable input power of 25 μW for implantable devices. Table I shows the SAR values and maximum allowable power. SAR was tested in the heart phantom and the HFSS homogeneous torso model. The higher numbers from the phantom are given. From the data presented, this design complies with IEEE requirements.

TABLE I
SAR AND MAXIMUM POWER VALUES.

1 g Peak SAR (W/kg)	10g Peak SAR (W/kg)	1 g net allowable power (mW)	10 g net allowable power (mW)
142.00	22.47	11.43	89.01

The communication link budget is assessed for connecting to patient smartphones. The link budget is calculated with the Friis transmission equations, similar to [20], [19] and [13]. The equations consider transmit antenna gain (G_t), receive antenna gain (G_r), and attenuation due to free space propagation (L). The carrier-to-noise density ratio (c/No) must be greater than 0 dB for communications and the equations assume line of sight. The following equations were used for calculating the link margin

$$\text{LM(dB)} = link\frac{c}{N_0}(dB) - required\frac{c}{\text{N}_0}(dB) \quad (2)$$

$$required\frac{c}{N_0} = \text{Eb} + 10\log_{10}(Br) - G_c + G_d \quad (3)$$

$$\text{link } \frac{c}{N_0} = \text{EIRP} - L_f + G_r - \text{N}_0 \quad (4)$$

$$\text{EIRP(dB)} = P_t + G_t \quad (5)$$

$$L_f = 20\log_{10}\frac{4\pi x}{\lambda} \quad (6)$$

where N_0 is the noise power density, E_b is the energy per bit, B_r is the bit rate, G_c is the coding gain, G_d is the fixing deterioration, $EIRP$ is the equivalent isotropically radiated power, L_f is the free space path loss, G_r is the receive gain,

P_t is the transmit power, G_t is the transmit gain, x is the transmission distance, and λ is the wavelength. Fig. 10 shows the link budget analysis where transmission is possible up to 7m. This would need to be validated with measurement of the fabricated antenna, as in the literature, measurement of the link budget is typically shorter range than in simulation [19]. Table II details the parameters for link budget analysis. Greater distance communication could be attained by increasing power to the regulation input limit or reducing the bit rate.

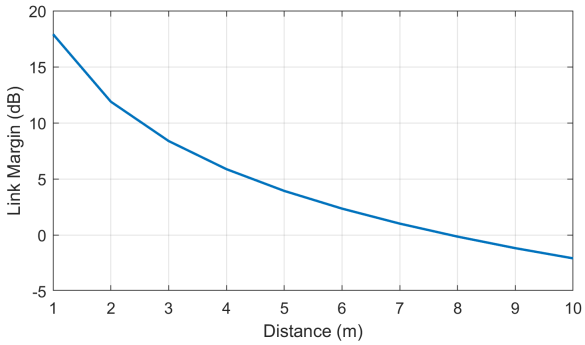

Fig. 10. The link margin of the proposed antenna at 2.45 GHz.

TABLE II
LINK BUDGET PARAMETERS.

G_t (dBi)	-34.7
P_t (dBm)	-36.5
G_r (dBi)	1.5
G_d (dB)	2.5
G_c (dB)	0
N_0 (dB/Hz)	-203.9
E_b /N_0 (dB)	9.6
B_r (Mb/s)	1

TABLE III
PROPOSED IMPLANTABLE ANTENNA COMPARED TO EXISTING LITERATURE. SIMULATED BANDWIDTH FOR [24] [20] AND [19] WERE ESTIMATED FROM PAPER FIGURES FOR COMPARISON.

Ref.	Type	Size (mm^3)	Freq. (GHz)	Sim. 10 dB BW (%)	Measured 10 dB BW (%)	Peak Gain (dBi)
[14]	Conformal	30×20.5×0.05	0.402	-	3.73	-32
[16]	Circular	π×6×0.64	0.402	-	6.94	-33.3
[13]	Conformal	6x6x0.254	1.4 2.45	-	17.1 12.8	-32.7 -25.9
[17]	Flat	7×6.5×0.375	0.4 1.6 2.45	-	36.8 10.7 8.9	-30.5 -22.6 -18.2
[26]	Flat	7×6×0.5	0.915 1.9 2.45	-	8.7 8.2 7.3	-26.4 -23 -20.5
[24]	Flat	3.45×3.4×0.5	2.45	4.9	10.6	-26.5
[19]	Flat	4×3×0.5	2.4	6.5	21.8	-25.9
[20]	Flat	3×3×0.5	2.45	7.0	22	-24.9
This Work	Flat	3×3×0.7	2.45	20.0	-	-34.7

Table III compares the proposed antenna with reported results in the literature. The antenna is compared by volume, frequency band, bandwidth and peak gain. The ultra-compact footprint of this antenna at 3x3x0.71 mm^3 is the second smallest in comparison to the literature [20]. In simulation, the proposed design shows a wide bandwidth in comparison to similar footprints [20] [19]. However, these authors report bandwidth widening of the fabricated antenna, measured in minced pork. Fabrication of the proposed design for real-world testing would have yielded a more direct comparison. Bandwidth widening in fabricated testing was observed in all the compared papers. This work's reported peak gain of -34.7 dBi is significantly worse than the gain values in the literature. However, the proposed antenna is still able to maintain a communication link. Through further optimisation of the design, it may be possible to improve the performance of the antenna in terms of gain and S11. It could also be possible to employ more miniaturisation techniques such as ground plane slots or multiple current paths. Simulation of the design could be improved by simulating in a heterogeneous human body model. However, many authors continue to real-world measurements of their design directly from homogeneous phantom optimisation [20]. Testing the design through fabrication and real-world measurements would improve the validity of the design. Measurements could include gain, S11 and the communication link testing in minced pork models, saline solution models and animal implantation.

IV. CONCLUSION

This communication presents a miniaturised antenna for leadless pacemaker systems operating in the 2.45 GHz ISM band. A size reduction to 3x3x0.71 mm^3 is realized through a high dielectric constant superstrate and a spiral meander structure. It was found that using a shorting pin in meander patch implantable antennas can increase the bandwidth in simulation, with a 20.0% ultra-wide bandwidth being achieved. The design exhibits a lower gain than many designs in the literature however, communication with patient smartphone devices was still possible up to 7m according to the link budget assessment. The ultra-compact antenna complies with SAR guidelines defined by IEEE C95.1-1999. Measurement of a fabricated device would need to be carried out with good agreement to simulation to validate the design. Further research could involve improving antenna performance through additional miniaturisation techniques such as ground plane modifications. The proposed antenna design elements could also be applied to other implantable devices or the wider field of antenna applications.

ACKNOWLEDGMENT

This work has made use of Hamilton HPC Service of Durham University.

This project has received funding from the European Union's Horizon 2020 research and innovation programme under the Marie Skłodowska-Curie grant agreement No 872172 (TESTBED2 project: www.testbed2.org).

REFERENCES

[1] R. Ibrahim, A. Khoury, and M. F. El-Chami, "Leadless pacing: Where we currently stand and what the future holds," *Current Cardiology Reports*, vol. 24, no. 10, pp. 1233–1240, Oct 2022. [Online]. Available: https://doi.org/10.1007/s11886-022-01752-y

[2] H. G. MOND and A. PROCLEMER, "The 11th world survey of cardiac pacing and implantable cardioverter-defibrillators: Calendar year 2009–a world society of arrhythmia's project," *Pacing and Clinical Electrophysiology*, vol. 34, no. 8, pp. 1013–1027, 2011. [Online]. Available: https://onlinelibrary.wiley.com/doi/abs/10.1111/j.1540-8159.2011.03150.x

[3] P. J. Bradshaw, P. Stobie, M. W. Knuiman, T. G. Briffa, and M. S. T. Hobbs, "Trends in the incidence and prevalence of cardiac pacemaker insertions in an ageing population," *Open Heart*, vol. 1, no. 1, 2014. [Online]. Available: https://openheart.bmj.com/content/1/1/e000177

[4] J. S. Guseh, *Aging of the World's Population*. John Wiley Sons, Ltd, 2015, pp. 1–5. [Online]. Available: https://onlinelibrary.wiley.com/doi/abs/10.1002/9781119085621.wbefs352

[5] P. L. C. L. d. L. L. L. F. W.-B. C. W. K. J. P. V. E. N. Nicolas Clémenty, Jérôme Fernandes and J.-C. Deharo, "Pacemaker complications and costs: a nationwide economic study," *Journal of Medical Economics*, vol. 22, no. 11, pp. 1171–1178, 2019, pMID: 31373521. [Online]. Available: https://doi.org/10.1080/13696998.2019.1652186

[6] K. Mountfort, R. Knops, J. Sperzel, and P. Neuzil, "The promise of leadless pacing: Based on presentations at nanostim sponsored symposium held at the european society of cardiology congress 2013, amsterdam, the netherlands, 2 september 2013," *Arrhythm Electrophysiol Rev*, vol. 3, no. 1, pp. 51–55, May 2014.

[7] L. Rosman, L. E. Rosenfeld, M. L. Johnston, and M. M. Burg, "Remote monitoring of implanted cardiac devices: A guide for patients and families," *Pacing and clinical electrophysiology*, vol. 41, no. 9, pp. 1224–1228, 2018.

[8] E. M. Cronin, J. C. Green, J. Lande, T. R. Holmes, D. Lexcen, and T. Taigen, "Performance of alert transmissions from cardiac implantable electronic devices to the CareLink network: A retrospective analysis," *Cardiovasc Digit Health J*, vol. 4, no. 3, pp. 72–79, Apr. 2023.

[9] K. G. Tarakji, A. M. Zaidi, S. L. Zweibel, N. Varma, S. F. Sears, J. Allred, P. R. Roberts, N. A. Shaik, J. R. Silverstein, A. Maher, S. Mittal, A. Patwala, J. Schoenhard, M. Emert, G. Molon, G. Augello, N. Patel, H. Seide, A. Porfilio, B. Maus, S. L. Di Jorio, K. Holloman, A. C. Natera, and M. P. Turakhia, "Performance of first pacemaker to use smart device app for remote monitoring," *Heart Rhythm O2*, vol. 2, no. 5, pp. 463–471, 2021. [Online]. Available: https://www.sciencedirect.com/science/article/pii/S2666501821001252

[10] C. Steinwender, P. Lercher, C. Schukro, H. Blessberger, G. Prenner, M. Andreas, J. Kraus, M. Ammer, and M. Stühlinger, "State of the art: leadless ventricular pacing : A national expert consensus of the austrian society of cardiology," *Journal of interventional cardiac electrophysiology : an international journal of arrhythmias and pacing*, vol. 57, no. 1, p. 27—37, January 2020. [Online]. Available: https://europepmc.org/articles/PMC7036055

[11] N. Bhatia and M. El-Chami, "Leadless pacemakers: a contemporary review," *J. Geriatr. Cardiol.*, vol. 15, no. 4, pp. 249–253, Apr. 2018.

[12] Vecteezy, "Cardiovascular vectors," *https://www.vecteezy.com/free-vector/cardiovascular, https://www.vecteezy.com/free-vector/heart-cross-section*, www.vecteezy.com.

[13] D. Sharma, B. K. Kanaujia, V. Kaim, R. Mittra, R. K. Arya, and L. Matekovits, "Design and implementation of compact dual-band conformal antenna for leadless cardiac pacemaker system," *Scientific Reports*, vol. 12, no. 1, p. 3165, Feb 2022. [Online]. Available: https://doi.org/10.1038/s41598-022-06904-2

[14] R. Das and H. Yoo, "Biotelemetry and wireless powering for leadless pacemaker systems," *IEEE Microwave and Wireless Components Letters*, vol. 25, no. 4, pp. 262–264, 2015.

[15] S. M. Asif, A. Iftikhar, B. D. Braaten, D. L. Ewert, and K. Maile, "A wide-band tissue numerical model for deeply implantable antennas for rf-powered leadless pacemakers," *IEEE Access*, vol. 7, pp. 31 031–31 042, 2019.

[16] M. Ramzan, A. Khaleghi, X. Fang, Q. Wang, N. Neumann, and D. Plettemeier, "An Ultra-Miniaturized high efficiency implanted spiral antenna for leadless cardiac pacemakers," *IEEE Trans Biomed Circuits Syst*, vol. 17, no. 3, pp. 621–632, Jul. 2023.

[17] I. A. Shah, M. Zada, and H. Yoo, "Design and analysis of a compact-sized multiband spiral-shaped implantable antenna for scalp implantable and leadless pacemaker systems," *IEEE Transactions on Antennas and Propagation*, vol. 67, no. 6, pp. 4230–4234, 2019.

[18] F. Faisal, M. Zada, H. Yoo, I. B. Mabrouk, M. Chaker, and T. Djerafi, "An ultra-miniaturized antenna with ultra-wide bandwidth for future cardiac leadless pacemaker," *IEEE Transactions on Antennas and Propagation*, vol. 70, no. 7, pp. 5923–5928, 2022.

[19] M. Zada, I. A. Shah, A. Basir, and H. Yoo, "Ultra-compact implantable antenna with enhanced performance for leadless cardiac pacemaker system," *IEEE Transactions on Antennas and Propagation*, vol. 69, no. 2, pp. 1152–1157, 2021.

[20] Y. Feng, Z. Li, L. Qi, W. Shen, and G. li, "A compact and miniaturized implantable antenna for ism band in wireless cardiac pacemaker system," *Scientific Reports*, vol. 12, 01 2022.

[21] M. Najafizadeh, S. Yazdi, M. Bozorg, M. Ghasempour-Mouziraj, M. Hosseinzadeh, A. Sarrafan, and P. Cavaliere, "2 - classification of ceramic coatings used in biomedical applications and their properties," in *Advanced Ceramic Coatings for Biomedical Applications*, ser. Elsevier Series in Advanced Ceramic Materials, R. K. Gupta, A. Motallebzadeh, S. Kakooei, T. A. Nguyen, and A. Behera, Eds. Elsevier, 2023, pp. 15–31. [Online]. Available: https://www.sciencedirect.com/science/article/pii/B9780323996266000032

[22] S. Mohammadi, A. Hedjazi, M. Sajjadian, N. Ghoroubi, M. Mohammadi, and S. Erfani, "Study of the normal heart size in northwest part of iranian population: a cadaveric study," *J Cardiovasc Thorac Res*, vol. 8, no. 3, pp. 119–125, Sep. 2016.

[23] S. Gabriel, R. W. Lau, and C. Gabriel, "The dielectric properties of biological tissues: Ii. measurements in the frequency range 10 hz to 20 ghz," *Physics in Medicine Biology*, vol. 41, no. 11, p. 2251, nov 1996. [Online]. Available: https://dx.doi.org/10.1088/0031-9155/41/11/002

[24] S. M. A. Shah, M. Zada, J. Nasir, O. Owais, and H. Yoo, "Electrically-small antenna with low sar for scalp and deep tissue biomedical devices," *IEEE Access*, vol. 10, pp. 90 971–90 981, 2022.

[25] M. Zada and H. Yoo, "Miniaturized dual band antennas for intra-oral tongue drive system in the ism bands 433 mhz and 915 mhz: Design, safety, and link budget considerations," *IEEE Transactions on Antennas and Propagation*, vol. 67, no. 9, pp. 5843–5852, 2019.

[26] ——, "A miniaturized triple-band implantable antenna system for bio-telemetry applications," *IEEE Transactions on Antennas and Propagation*, vol. 66, no. 12, pp. 7378–7382, 2018. [Online]. Available: https://doi.org/10.1109/TAP.2018.2874681